# Parity-dependent rotational rainbows in $D_2$–NO and He–NO differential collision cross sections

Arjan Gijsbertsen
*Laser Centre and Department of Physical Chemistry, Vrije Universiteit Amsterdam, De Boelelaan 1083, 1081 HV Amsterdam, The Netherlands*

Harold Linnartz
*Sackler Laboratory for Astrophysics, Leiden Observatory, P.O. Box 9513, 2300 RA Leiden, The Netherlands*

Steven Stolte[a)]
*Laser Centre and Department of Physical Chemistry, Vrije Universiteit Amsterdam, De Boelelaan 1083, 1081 HV Amsterdam, The Netherlands*

(Received 25 April 2006; accepted 27 June 2006; published online 4 October 2006)

The $(j',\bar{\Omega}',\epsilon')$ dependent differential collision cross sections of $D_2$ with fully state selected ($j=1/2$, $\Omega=1/2$, $\epsilon=-1$) NO have been determined at a collision energy of about 550 $cm^{-1}$. The collisionally excited NO molecules are detected by $(1+1')$ resonance enhanced multiphoton ionization combined using velocity-mapped ion-imaging. The results are compared to He–NO scattering results and tend to be more forward scattered for the same final rotational state. Both for collisions of the atomic He and the molecular $D_2$ with NO, scattering into pairs of rotational states with the same value of $n=j'-\epsilon\epsilon'/2$ yields the same angular dependence of the cross section. This "parity propensity rule" remains present both for spin-orbit conserving and spin-orbit changing transitions. The maxima in the differential cross sections—that reflect rotational rainbows—have been extracted from the $D_2$–NO and the He–NO differential cross sections. These maxima are found to be distinct for odd and even parity pair number $n$. Rainbow positions of parity changing transitions ($n$ is odd) occur at larger scattering angles than those of parity conserving transitions ($n$ is even). Parity conserving transitions exhibit—from a classical point of view—a larger effective eccentricity of the shell. No rainbow doubling due to collisions onto either the N-end or the O-end was observed. From a classical point of view the presence of a double rainbow is expected. Rotational excitation of the $D_2$ molecules has not been observed. © *2006 American Institute of Physics*. [DOI: 10.1063/1.2234771]

## I. INTRODUCTION

Crossed molecular beam machines[1] provide an important tool towards a better understanding of the dynamics of chemical elementary processes.[2,3] These machines allow experimentalists to study the outcome of (gas phase) encounters of molecules with atoms and/or other molecules under well defined conditions (collision energy and initial state of the colliding molecules). All chemical reactions consist of a large number of elementary chemical processes that must be studied at an atomic/molecular level of detail to understand macroscopic chemical reactions and energy transfer. Steering these reactions is a long-standing goal in molecular sciences and for this it is necessary to understand and to predict the outcome of a single molecular encounter.

Since the pioneering work of Lee, Polanyi, and Herschbach, an enormous progress in the field of reaction dynamics has been achieved. An important development has been the introduction of the ion-imaging technique.[4] This method allows one to record the whole [two-dimensional (2D)] velocity distribution of reaction products in a single measurement. The velocity-mapped ion-imaging technique,[5,6] that uses electrostatic lenses to project the velocity distribution onto the detector, is nowadays a common tool in the field of molecular dynamics.[6–11]

In the past, several reaction dynamical studies—both experimental and theoretical—have focused on the rotationally inelastic scattering of NO with a number of collision partners.[8,10,12,13] The main reason for this is that NO is both an interesting and convenient model system. It is a radical, with nonzero angular momentum in its rotational ground state, while it is stable enough to be stored in a gas bottle. Furthermore, it is easily detected with spectroscopic methods such as laser induced fluorescence[14] (LIF) and resonance enhanced multiphoton ionization[10,15] (REMPI). Using the hexapole focusing technique,[16] NO can be fully selected into a single quantum state (upper component of the $\Lambda$ doublet) as it undergoes a first order Stark effect.[17] The two components of the $\Lambda$ doublet within the same rotational level have opposite parities, but only a minute energy splitting. Parity propensity effects for Hund's case (a) molecules are far more important than the effects of the orientation of the unpaired electron charge cloud. The latter effects are responsible for the $A'$ and $A''$ symmetries of the potential energy surfaces (PESs).[12] By (hexapole) selection of NO in a single quantum

[a)]Author to whom correspondence should be addressed. Fax: +31-20-4447643. Electronic mail: stolte@few.vu.nl

 

state before collision, the effect of parity changing and parity conservation on the differential cross section can be isolated from the effect of the excitation energy.

It was shown recently, that interesting physical effects emerge for inelastic He–NO scattering experiments when full (hexapole) state selection is applied.[18] The angular dependence of the cross section for excitation to pairs of states with the same parity was noted to be similar. In the present study we will assess this effect quantitatively, by a direct comparison of the differential cross sections for two different systems. This parity propensity follows directly from a simple quasi-quantum-mechanical treatment (QQT),[19] which also provided some new insights into the orientation dependence of the inelastic collision cross section.

In our search towards a better understanding of inelastic collisions, additional velocity-mapped ion-imaging measurements on $D_2$–NO inelastic scattering have been performed. This collision system is very close to He–NO, but still distinguishable[20] and provides thus valuable information about the effect of a small difference of the interaction potential on the differential cross section. In the current work, we focus on "parity pairs" and the position of the rotational rainbows. Classical rotational rainbows[21] are reflected by the maxima in the rotationally inelastic scattering angular distributions.

## II. EXPERIMENT

The experimental setup has been described in detail in Ref. 18 and only the most relevant conditions are mentioned here. A beam of 16% NO seeded in Ar expands from a general valve, which forms the first step of state selection. Due to adiabatic cooling, most of the NO molecules are in their rotational ground state with rotational quantum number $j=1/2$. Via two skimmers, the NO beam enters a 1.6 m long hexapole. The hexapole focuses molecules in the low field seeking upper component of the $\Lambda$ doublet ($j=1/2$, $\bar{\Omega}=1/2$, $\epsilon=-1$) into the collision region and diverges molecules in the lower component ($j=1/2$, $\bar{\Omega}=1/2$, $\epsilon=1$). The parameter $\epsilon$ denotes the symmetry index, while $\bar{\Omega}$ ($=|\Omega|$) is the projection (absolute value of the projection) of the electronic angular momentum onto the molecular axis. Molecules in higher rotational states are much less affected by the hexapole and the resulting divergence of the molecular beam over the 3 m distance from nozzle to collision region reduces the relative amount of molecules in higher rotational states in the beam by approximately a factor of 70 (hexapole gain of the focused state).

The hexapole focused beam of NO molecules ($v_{NO}=593$ m/s) is crossed in the collision chamber by a beam of $D_2$ molecules ($v_{D_2}=1830$ m/s).[20] These velocities result in a nominal collision energy of 550 $cm^{-1}$, which is slightly larger than in the case of He–NO scattering (514 $cm^{-1}$).[18] An encounter of a $D_2$ molecule with a NO molecule can in principle induce rotation of the NO and/or the $D_2$ molecule. Energetically it is allowed to excite the NO molecules up to $\Delta j=j'-j=16$ while the $D_2$ molecules can be excited up to $\Delta j=4$. The rotationally excited NO molecules are ionized via a $(1+1')$ REMPI scheme[15] along the electronic $A\,^2\Sigma^+ \leftarrow X\,^2\Pi$ transition using an excimer (XeCl) pumped dye laser with a bandwidth of about 0.1 $cm^{-1}$. Velocity-mapped ion imaging is applied to obtain the two dimensional velocity distribution of the scattered NO molecules.

To suppress contributions from other ionized molecules (oil or water) to the ion images, time-of-flight (TOF) gating is applied. The contributions to the images of thermal NO and of noncolliding molecules in the NO beam at the collision center are minimized by subtracting background images. The $D_2$ beam is switched from "on" to "off" after each 100 laser shots. This procedure is repeated typically 20 times. The images with the $D_2$ beam off are subtracted from those with the $D_2$ beam on. As the excimer/dye laser system and general valves run at 10 Hz, collecting an image takes approximately 7 min. Because of low signal, some of the highest rotational states ($\Delta j>10$) required twice the integration time.

Differential cross sections are extracted from the ion images following the extraction procedure described in Ref. 18. In this procedure, collision-induced rotational alignment, the detection probability due to different residence times for slow and fast molecules within the detection volume, and blurring of the images are explicitly taken into account. An empirical blurring factor is used to make the simulated images as sharp as the experimental ones. To correct for alignment, the assumption is used that the projection $m_a$ of the rotational angular momentum $\boldsymbol{j}$ on the kinematic apse is conserved. The alignment dependent correction accounts for (partial) saturation.

## III. RESULTS AND DISCUSSION

### A. Differential cross sections and parity pairs

A set of (raw) velocity-mapped ion images for spin-orbit conserving collisions[33] ($\bar{\Omega}=\bar{\Omega}'=1/2$) is plotted in Fig. 1. The projected Newton sphere is cylinder symmetric around the relative velocity ($v_{rel}=v_{D_2}-v_{NO}$). The camera is oriented such that $v_{NO}$ points from right to left, while $v_{D_2}$ points from the top to the bottom of the images. The resulting orientation of $v_{rel}$ is from top left to bottom right.

The intensity on an outer ring of an ion image (on both sides of $v_{rel}$) gives a first impression of the differential cross section. Note that the intensity on the top-left part of the images is due to forward scattered molecules, while backward scattered molecules are detected at the lower-right part of the image. In the images it is clearly seen that forward scattering is preferred for NO scattering into low rotational states, while for high final rotational states backward scattering dominates. The ion images for spin-orbit changing transitions ($\bar{\Omega}'=3/2$) are not shown in this work, but are of a similar quality as those in Fig. 1. Rotational excitation of the $D_2$ molecules is not observed in the ion images. This should show up as small projected Newton sphere dominated by backward scattering in the images for low rotational states of the NO molecules.

For He–NO collisions[18] it was found that scattering—at the same value of $j'$—into the upper component of the $\Lambda$ doublet ($\epsilon=-1\rightarrow\epsilon'=-1$) yields more forward scattering

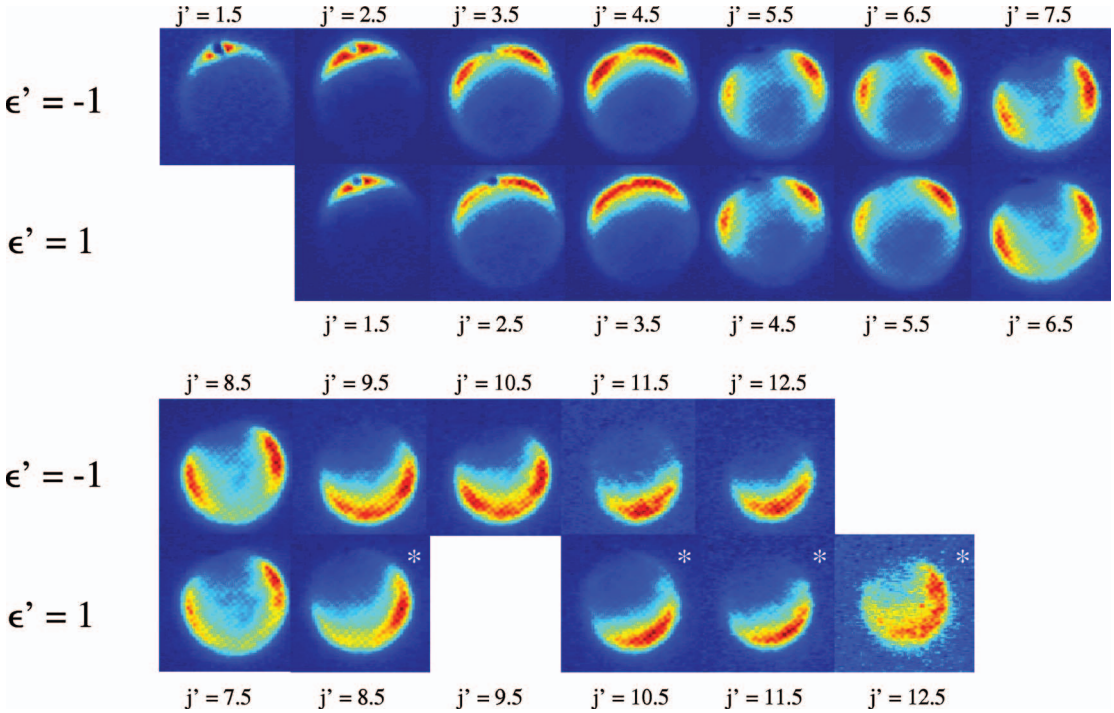


FIG. 1. (Color) Set of raw experimental ion images for spin-orbit conserving ($\bar{\Omega}=\bar{\Omega}'=1/2$) $D_2$–NO scattering. The images for $\epsilon'=-1$ are collected using the $R_{21}$ spectroscopic branch. The majority of the images for $\epsilon'=1$ are collected via the $P_{11}$ branch; those labeled with a star ( $^*$) are from the combined $R_{11}+Q_{21}$ branch that exhibits more asymmetry with respect to the $v_{\mathbf{rel}}$. This is due to the combination of collision-induced alignment and the residence time of the molecules in the detection region. For a $P$ and $R$ branch transition the effects of alignment and residence time nearly cancel, while for $Q$ branch transitions these add, yielding very asymmetric ion images. The images are plotted such that two images above each other relate to the same parity pair $n=j'+\epsilon'/2$. The missing image for $j'=9.5$, $\epsilon'=1$ could not be collected due to overlapping spectral lines.

than into the lower component of the Λ doublet ($\epsilon=-1 \rightarrow \epsilon'=1$). Such a difference is also found in the present $D_2$–NO images.

Scattering into the lower component of the Λ doublet seems to be "one rotational quantum ahead" of scattering into the upper component of the Λ doublet. For example, similar images are collected for excitation to the $j'=4.5$, $\epsilon'=1$ and the $j'=5.5$, $\epsilon'=-1$ states, as is the case for the $j'=5.5$, $\epsilon'=1$ and the $j'=6.5$, $\epsilon'=-1$ states, etc. This similarity holds both for spin-orbit conserving and spin-orbit changing transitions. Note that these final states carry the same parity and for this reason the pairs are referred to as "parity pairs." The parity for a rotational state $j,\epsilon$ follows from

$$p=(-1)^{j-\epsilon/2}. \tag{1}$$

The parity of a rotational state relates to the symmetry properties of its wave function $\psi(\boldsymbol{r})$ and is defined by its behavior under parity transformation (inversion), which acts as an operator $\boldsymbol{P}$ on a wave function $\psi$:

$$\boldsymbol{P}\psi(\boldsymbol{r})=\psi(-\boldsymbol{r})=p\psi(\boldsymbol{r}). \tag{2}$$

Note that $\boldsymbol{r}$ represents here both electronic and nuclear coordinates.

To illustrate the presence of parity pairs, the images in Fig. 1 are plotted such that two images above each other belong to the same pair. The parity pairs are numbered as

$$n=j'-\frac{\epsilon\epsilon'}{2}, \tag{3}$$

which reduces in our experiment to $n=j'+\epsilon'/2$ as $\epsilon=-1$. Figure 2 provides a schematic representation of the NO energy levels including the parity pair number $n$ for the (current experimental) case $j=1/2$, $\epsilon=-1$. The physical background of pairs with these labels is discussed in detail in Ref. 19. The integral that leads to the differential cross section contains a phase shift factor and a Legendre polynomial $P_{j'-\epsilon\epsilon'/2}$. If the energy spacing between the rotational levels is small, the phase shift factor has little influence. Because of the Legendre polynomial, excitation to a pair of rotational states with the same label $n$ should show a similar angular dependence of the cross section. Even Legendre polynomials contribute to parity conserving transitions, while odd Legendre polynomials contribute to parity breaking transitions.

In the case of NO the electron cloud of the unpaired electron is nearly cylinder symmetric with respect to the internuclear axis [Hund's case(a)]. The mixing between $\bar{\Omega}=3/2$ and $\bar{\Omega}=1/2$ is small, so the angular distribution of an $\epsilon=1\rightarrow\epsilon'=-1$ transition is nearly equal to that of $\epsilon=-1 \rightarrow \epsilon'=1$ and the angular distribution of an $\epsilon=-1\rightarrow\epsilon'=-1$ transition is nearly equal to that of $\epsilon=1\rightarrow\epsilon'=1$.

The $D_2$–NO differential cross sections that are extracted from the images (indicated in the figures as "dcs") are shown in Fig. 3. The extracted cross sections for spin-orbit changing collisions ($\bar{\Omega}'=3/2$) are shown in Fig. 4. Tables with $D_2$–NO differential cross sections are available online.[34] To

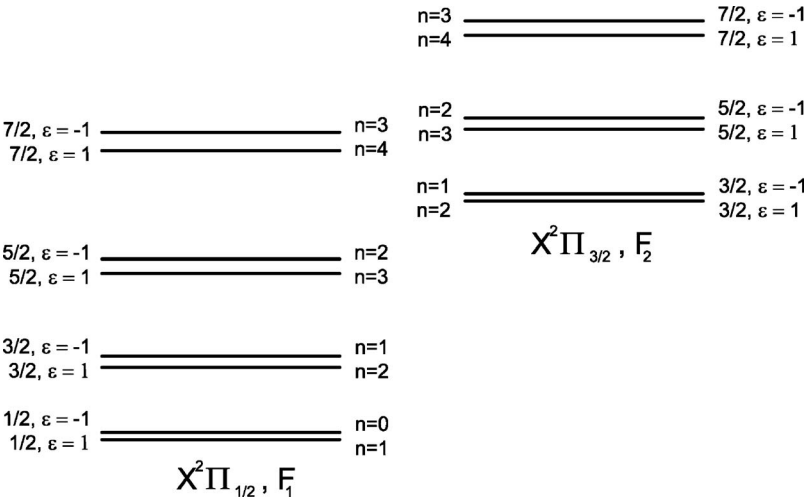


FIG. 2. The rotational levels of the NO molecule are labeled with their rotational quantum number $j$ and symmetry index $\epsilon=\pm 1$. Recall that parity $p$ and $\epsilon$ relate as $p=(-1)^{j-\epsilon/2}$. The parity pair numbers $n$ in this figure relate to the experimental case where the incoming state is given by $j=1/2$, $\epsilon=-1$. Parity pairs are observed for both spin-orbit conserving as for spin-orbit changing transitions, but the differential cross sections of a parity pair $n$ for spin-orbit conserving transitions does not correspond to that of the same pair $n$ for a spin-orbit changing collision. The energy differences are taken arbitrarily and are not scaled to the actual values.

illustrate the pairwise structure, the differential cross sections that form a pair are plotted in the same panel. Those for excitation to the $j'=12.5$ states of the $\epsilon'=1$ state are plotted separately in Fig. 5. For the purpose of comparison, all differential cross sections are normalized with respect to each other such that the integral $\int \mathrm{dcs}\, d\vartheta=1$. Note that this is not the usual integral cross section ($\int \mathrm{dcs} \sin\vartheta d\vartheta$). Normalization on the total cross section suppresses information for scattering angles close to 0° and 180°. As we focus on the shape of the differential cross section all scattering angles are equally important. The plotted cross section is the average of two experimental results if two spectroscopic branches were available to collect data.

An interesting observation in Fig. 5 is that—opposite to what one would expect from a classical point of view—the cross sections for scattering into the $j'=12.5$, $\Omega'=1/2$, $\epsilon'=1$ is more or less dominated by sideways scattering. This effect has been observed to be even more pronounced for He–NO scattering, but no satisfactory explanation is available yet. If we extrapolate the observed pairwise structure,

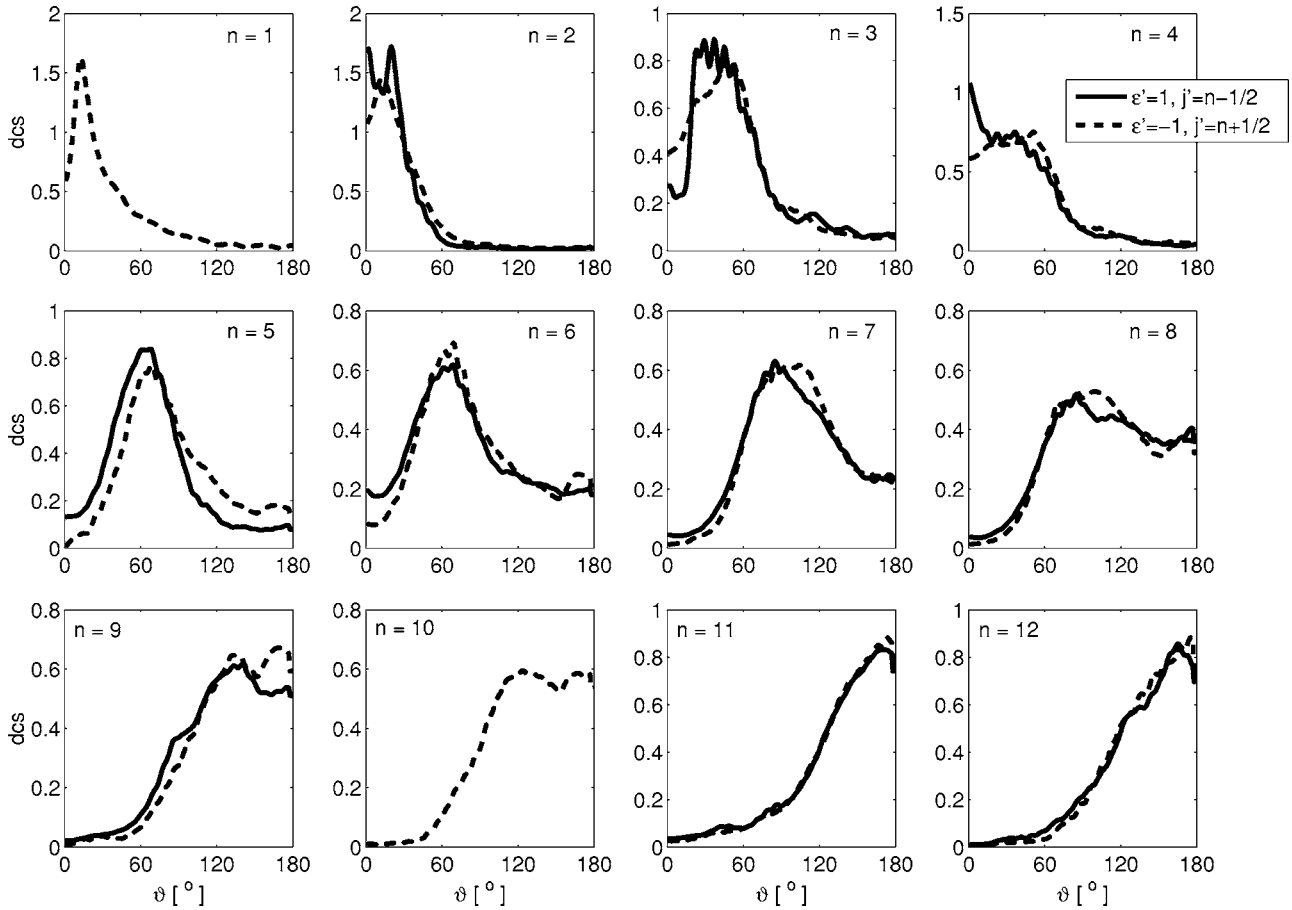


FIG. 3. Differential cross sections for ($D_2$–NO) scattering into $\bar{\Omega}'=1/2$. The differential cross sections are plotted per parity pair and normalized such that the integral $\int \mathrm{dcs}\, d\vartheta=1$. The differential cross section for $j'=12.5$, $\epsilon'=1$ is plotted separately in Fig. 5.

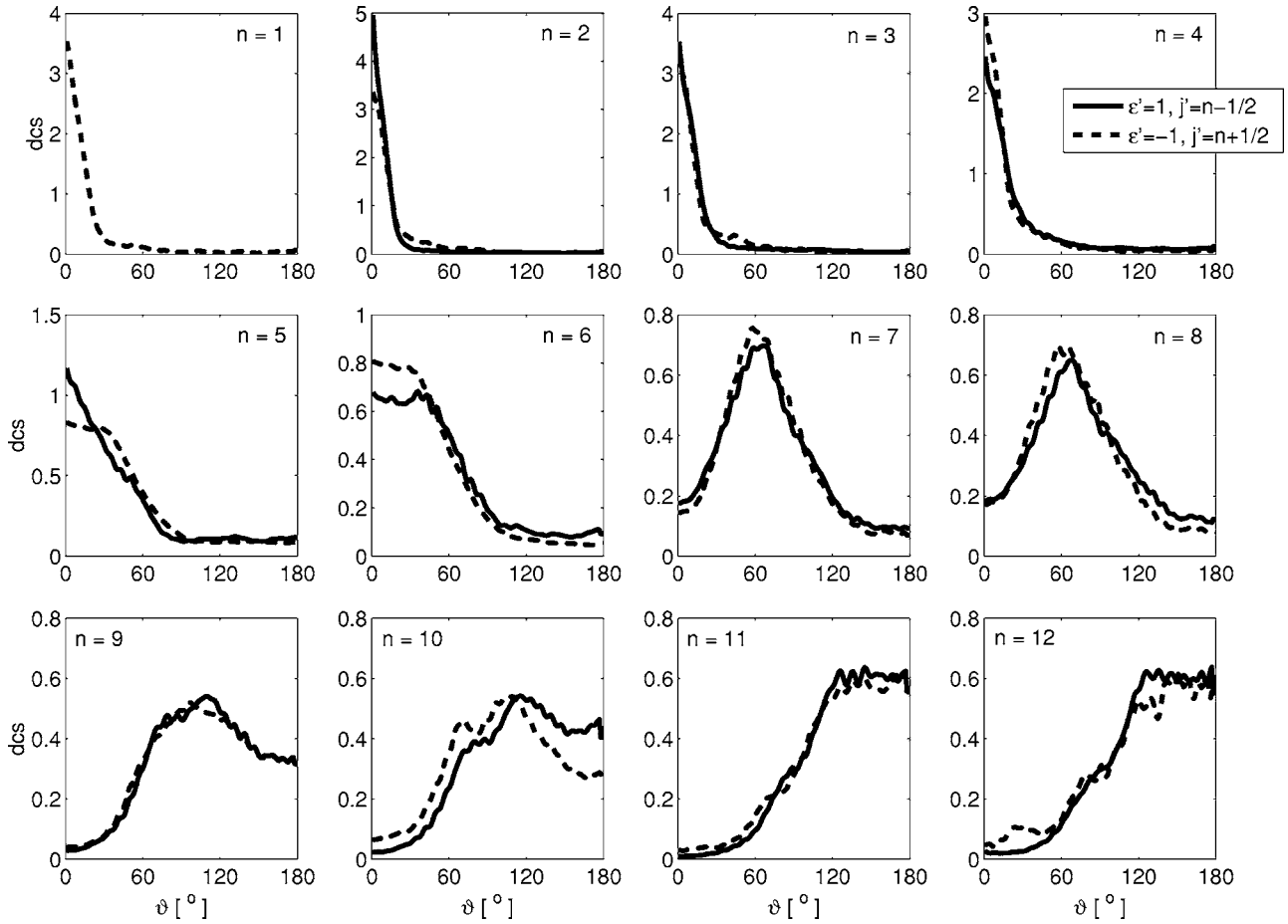


FIG. 4. Differential cross sections for ($D_2$–NO) scattering into $\bar{\Omega}'=3/2$. The differential cross sections are plotted per parity pair and normalized such that the integral $\int \mathrm{dcs}\, d\vartheta=1$. The differential cross section for $j'=12.5$, $\epsilon'=1$ is plotted separately in Fig. 5.

the differential cross section for the $j'=12.5$, $\Omega'=1/2$, $\epsilon'=1$ should be similar to that of the $j'=13.5$, $\Omega'=1/2$, $\epsilon'=-1$ final rotational state. This latter state is classically not allowed. Energetically it is, but the maximally applied torque is too small to allow for such a high rotational state.[22] Quantum mechanically these transitions are allowed, but with a much smaller cross section.

Experimental differential cross sections (as published in Ref. 18) for He–NO collisions are plotted (grouped per parity pair) in Figs. 6 and 7 to show the presence of parity pairs and to allow for a systematic comparison with those for $D_2$–NO scattering in Figs. 3 and 4. In agreement with the close coupling (CC) calculations[18] of the He–NO differential cross sections, the angular dependences of the experimental cross sections within a parity pair $n$ are remarkably similar for both collision systems.

In addition to parity pairs $n$ of the differential cross sections of $D_2$–NO and He–NO, as plotted in Figs. 3–7 there

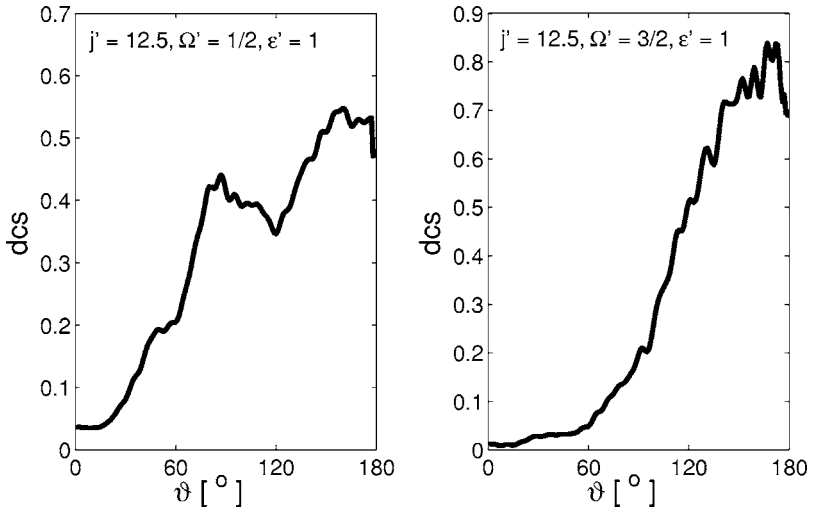


FIG. 5. Differential cross sections for ($D_2$–NO) scattering into the highest observed rotational state $j'=12.5$ of the lower component of the $\Lambda$ doublet ($n=13$). Note that the differential cross section for $\Omega'=1/2$, $\epsilon'=1$ has a strong sideways scattered contribution. From a simple classical model this cannot be understood. A similar, but even more pronounced effect has been observed for He–NO collisions (Ref. 18).

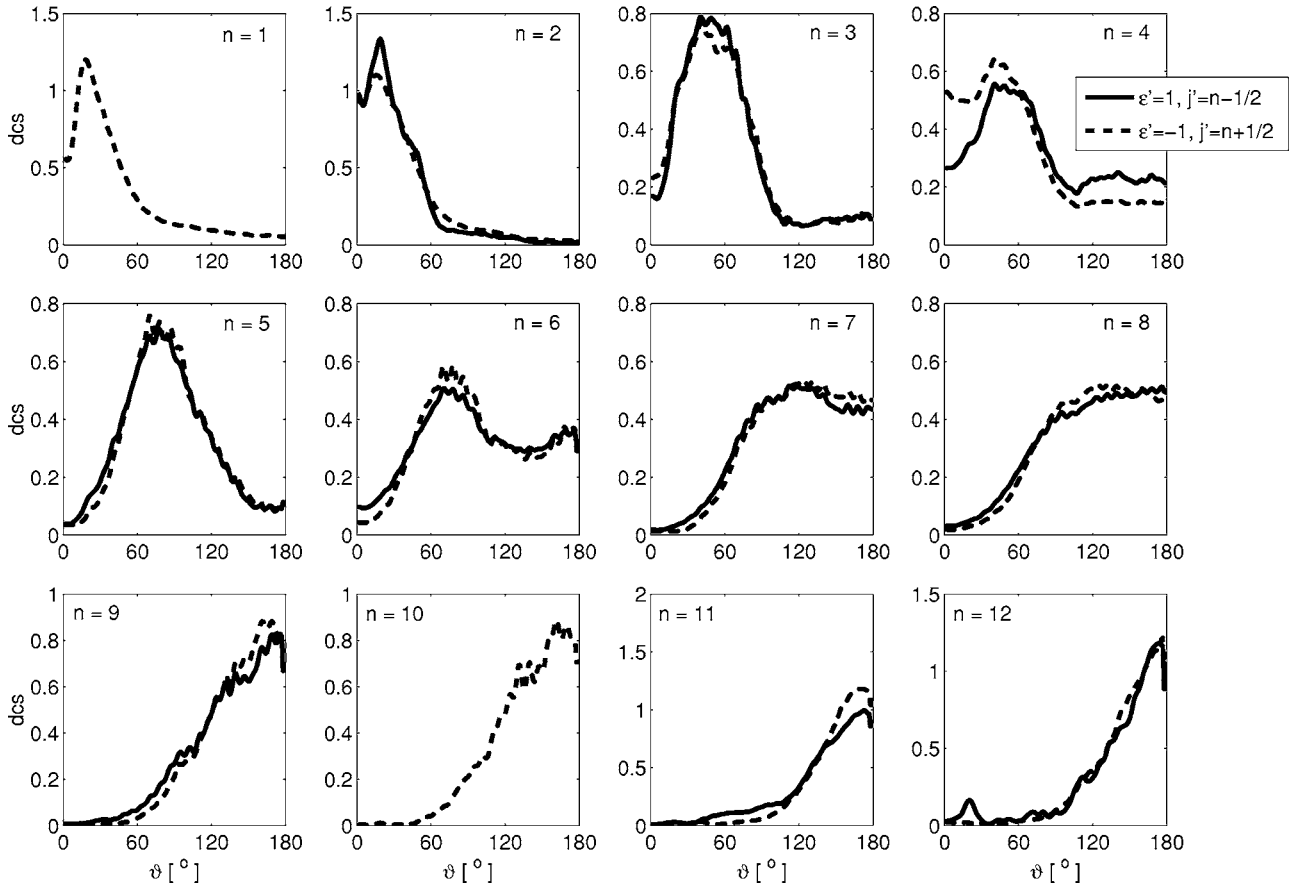


FIG. 6. Differential cross sections for (He–NO) scattering into $\Omega'=1/2$. The differential cross sections are plotted per parity pair and normalized such that the integral $\int \mathrm{dcs}\, d\vartheta=1$.

is also some resemblance between the differential cross sections of $n=1$ and $n=2$, of $n=3$ and $n=4$, etc. These pairs can be labeled via $k$, where $k=n/2$ if $n=$"even" and $k=(n+1)/2$ if $n=$"odd". See for an example of such a pair the images for $j'=4.5$, $\epsilon'=1$ and $j'=5.5$, $\epsilon'=1$. Although the images turn out to be quite similar for these cases, significant differences between the resembling differential cross sections are present. For excitation to states with $n=$even slightly more forward scattering is observed than for $n=$odd. This becomes most clear in the cross sections for $n=5$ and $n=6$ in Fig. 6.

Upon a close inspection of the details of Figs. 3–7 one notices imperfections that can mostly be attributed to statistical uncertainties in the ion images. Especially in the near forward direction the differential cross sections are often imperfect due to background subtraction and due to diffraction which shows up as a rapid oscillation beyond our angular resolution. These oscillations contribute only for $n\leqslant 4$ as can be seen in the CC results of Ref. 18. The false maximum in the backward direction ($\vartheta$ very close to 180°) can be caused by a small inaccuracy in the extraction procedure. Overall there is excellent agreement between the differential cross sections within each parity pair.

### B. Rotational rainbows

At first sight, there is not much difference between the differential cross sections for He–NO and $D_2$–NO. Both cases clearly exhibit the pairwise behavior and range from forward to backward scattering when $\Delta j$ is raised. The $D_2$–NO cross sections are slightly more forward scattered than those of He–NO. The scattering angles at which the measured differential cross sections of He–NO and $D_2$–NO reach their maximum angle $\vartheta_m$ are plotted in Fig. 8 as a function of the parity pair number $n$. These maxima $[\vartheta_m(n)]$ reflect the classical rotational rainbow angles $[\vartheta_r(\Delta J)]$. Here $\Delta J$ is the (classical) continuous equivalent of the quantum step $\Delta j$. The angle $\vartheta_r(\Delta J)$ corresponds to the minimum scattering angle at which a specific amount of incoming translational momentum is transformed into molecular rotation. At $\vartheta=\vartheta_r(\Delta J)$, the classical (double) differential cross section $d^2\sigma/d\omega d\Delta J$ becomes singular. This can be understood by considering the scattering from a (nonrotating) nearly convex hard shell.[22] A schematic representation of such a hard shell scattering process is shown in Fig. 9.

The initial conditions at which $\Delta J$ is transferred into rotation are uniquely defined when one specifies $\gamma_n$: the angle between the surface normal $\hat{\boldsymbol{n}}$ and the molecular axis $\hat{\boldsymbol{r}}$ at the impact position of the atom onto the molecular shell. The incoming momentum is given by $\boldsymbol{p}=\mu v_{\mathbf{rel}}$, with $\mu$ the reduced mass and $v_{\mathbf{rel}}$ the relative velocity of the system. At the point of impact $\boldsymbol{R}_s$, the perpendicular component of the incoming momentum $\boldsymbol{p}_\perp=(\boldsymbol{p}\cdot\hat{\boldsymbol{n}})\hat{\boldsymbol{n}}$ is responsible for $\Delta J$. The perpendicular component of the momentum after collision $\boldsymbol{p}'_\perp$ points opposite to that before collision: $\hat{\boldsymbol{p}}'_\perp=-\hat{\boldsymbol{p}}_\perp$. The

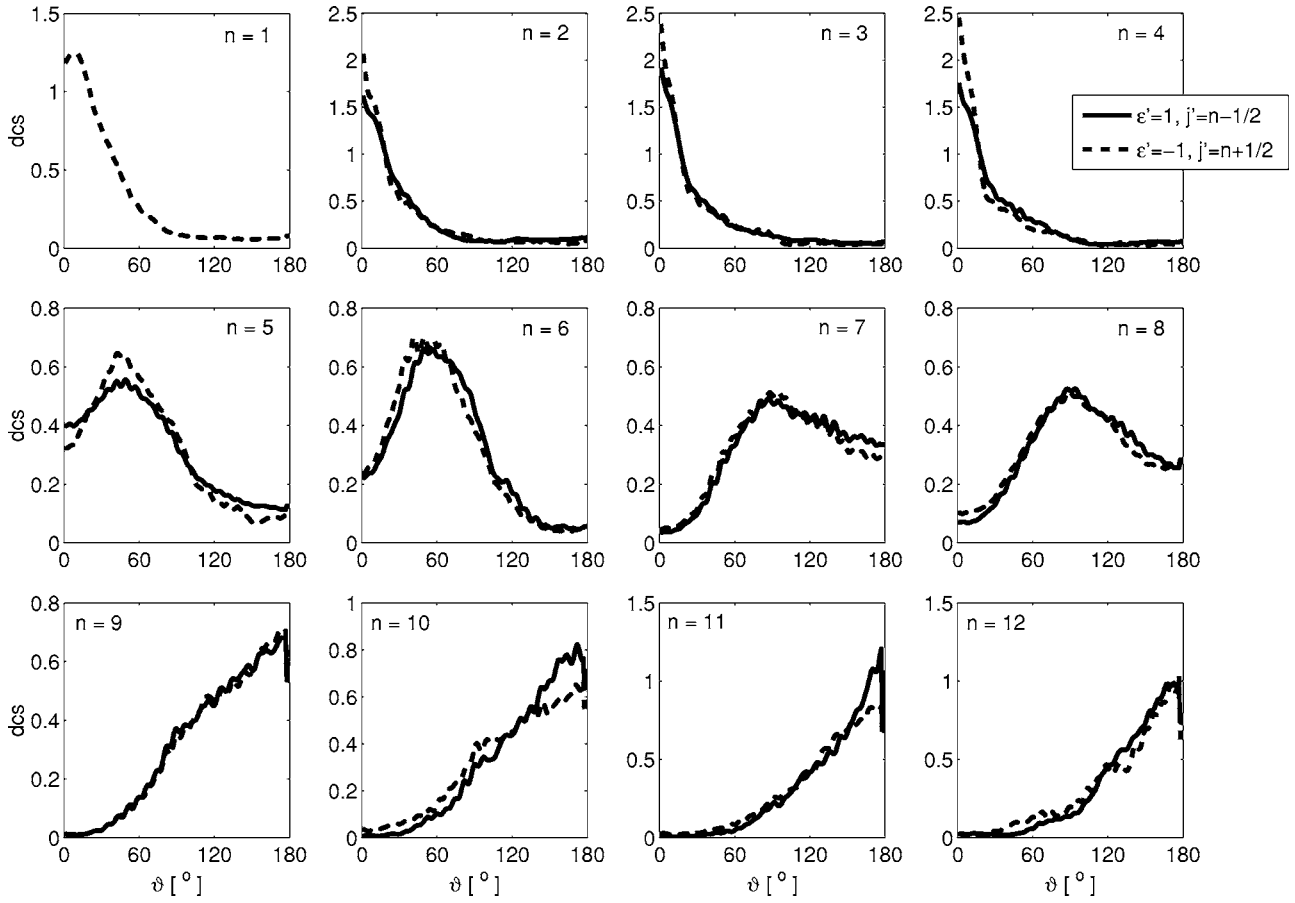


FIG. 7. Differential cross sections for (He–NO) scattering into $\Omega'=3/2$. The differential cross sections are plotted per parity pair and normalized such that the integral $\int \mathrm{dcs}\, d\vartheta=1$.

parallel component of the momentum $\boldsymbol{p}_\parallel=\boldsymbol{p}-\boldsymbol{p}_\perp$ remains conserved during the collision $\boldsymbol{p}'_\parallel=\boldsymbol{p}_\parallel$. The magnitude of the rotational excitation is proportional to the effective impact parameter $b_n$ at the point of impact.[23] This impact parameter is the shortest distance between the surface normal and the center of mass of the molecule.

For a convex shell, there are three values of $\gamma_n$ at which $b_n=0$: two at each end of the molecule ($\gamma_n=\gamma_R=0,\pi$) and one near the equator ($\gamma_n=\gamma_R\approx\pi/2$). The angle $\gamma_R$ depicts the position vector of the shell $\boldsymbol{R}_s$ with respect to the center of mass of the molecule. In between these zero positions of $b_n$ there are two maximum values, one on each side of the molecule, that allow for maximum rotational excitation.[24] In the case of an ellipsoid[23] this is at $b_n=A-B$ where $A$ and $B$ are its major and minor axis, respectively. All together this implies that there are (except at $b_n=0$ and at its maximum value) four angles ($\gamma_n$) that lead to the same value of $b_n$.

From conservation of energy and angular momentum it can be shown that

$$k_\perp \equiv p_\perp/\hbar = \frac{1+\mu_n^2(\gamma_n)/I}{2b_n(\gamma_n)}\Delta J, \tag{4}$$

$$k'_\perp = \sqrt{k_\perp^2 - \mu\Delta J^2/I}, \tag{5}$$

where $I$ is the moment of inertia of the molecule. At fixed values of $\Delta J$ and incoming momentum $k$, the smallest scattering angle occurs at the maximum value of $b_n$. Note that since $k_\parallel$ is conserved, the scattering angle $\vartheta$ increases with $k_\perp$. At backward scattering ($\vartheta=180°$), the substitution of $k=k_\perp$ determines the lower limit of $b_n$ for which this transition is possible. The scattering angle $\vartheta$ relates to $\boldsymbol{k}$ as

$$\vartheta = \arctan\left(\frac{k_\perp}{k_\parallel}\right) + \arctan\left(\frac{k'_\perp}{k_\parallel}\right). \tag{6}$$

Four values of $\gamma_n$ (leading to the same value of $b_n$) contribute to $d^2\sigma/d\omega d\Delta J$ at the same scattering angle $\vartheta$. In general, the differential cross section becomes the sum over these four contributions:

$$\frac{d^2\sigma}{d\omega d\Delta J} \propto \sum_{i=1}^{4}\frac{d^2\sigma(\gamma_{n,i})}{d\omega d\Delta J} = \sum_{i=1}^{4}\frac{d^2\sigma(\gamma_{n,i})}{d\omega_n d\Delta J}\frac{d\omega_n}{d\omega}. \tag{7}$$

Note that $d\omega=\sin\vartheta d\vartheta d\varphi$ and $d\omega_n=\sin\gamma_n d\gamma_n d\varphi_n$.

A singularity in the (double) differential cross section appears when $d\omega/d\omega_n=0$. This derivative can be expressed as

$$\frac{d\omega}{d\omega_n} \propto \frac{\sin\vartheta}{\sin\gamma_n}\frac{d\vartheta}{d\gamma_n} = \frac{\sin\vartheta}{\sin\gamma_n}\frac{d\vartheta}{db_n}\frac{db_n}{d\gamma_n}. \tag{8}$$

The singularity occurs if $db_n/d\gamma_n=0$; in other words, for collisions onto the two maximum values of the effective impact parameter. The classical differential cross section for a specific value of $\Delta J$ at its smallest scattering angle ($\vartheta_r$) will

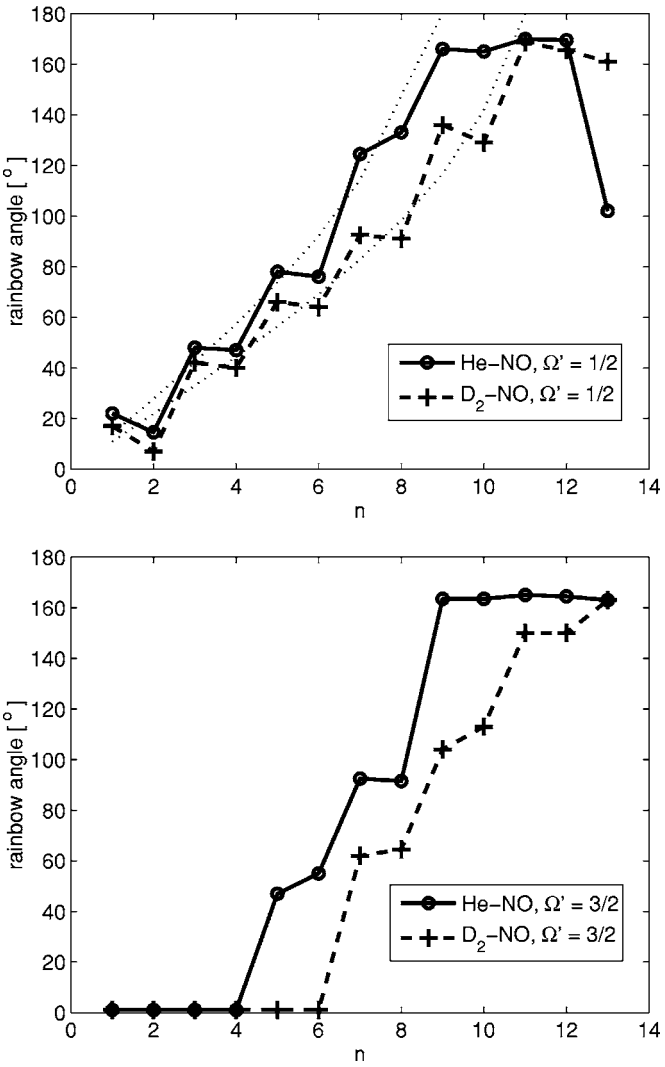


FIG. 8. The positions of the rotational rainbows for each parity pair $j'+\epsilon'/2$ are plotted for both $D_2$–NO and He–NO scattering. The upper panel shows the rainbow maxima for spin-orbit conserving ($\Omega'=1/2$) collisions, while the lower panel shows the rainbow maxima for spin-orbit changing ($\Omega'=3/2$) collisions. The results are averaged over both components of the pairs. To guide the eyes, the points for He–NO and $D_2$–NO are connected via lines. The dotted line in the upper panel follows from a fit of parameters $A$ and $B$ of Eq. (9) to the data points.

approach infinity. For the special case of an ellipsoid hard shell, the rotational rainbow angle $\vartheta_r$ takes place at[23]

$$\sin\left(\frac{1}{2}\vartheta_r\right)=\frac{\Delta J}{2k(A-B)}. \tag{9}$$

Previous theoretical studies[25–27] at comparable collision energies and similar anisotropic systems conclude that the classical rotational rainbow angle $\vartheta_r$ is usually substantially smaller than the scattering angle found for maximum scattered intensity. This effect is especially pronounced at large scattering angles.

To extract $\theta_m$, the scattering angle of the maxima from the experimental results, the differential cross sections (in Figs. 3–7) were smoothed. A zero-phase (forward and reverse) filtering routine was applied to remove fast oscillations in the differential cross sections. Differential cross sections obtained from three ion images (for $D_2$–NO with $j'=3.5$, $\Omega'=1/2$, $\epsilon'=1$, for $D_2$–NO with $j'=9.5$, $\Omega'=1/2$, $\epsilon'=-1$, and for He–NO with $j'=7.5$, $\Omega'=1/2$, $\epsilon'=1$) were omitted, mainly because of experimental inaccuracies. The decision to leave these cross sections out was based on three criteria: the maxima of the extracted differential cross sections are (1) far away from the result via a different spectroscopic branch, (2) far away from the corresponding theoretical value,[18] and (3) far away from the rainbow maximum of the differential cross sections for other final rotational states within a parity pair. These experimental differential cross sections are nevertheless included in (the calculations for) Figs. 3–7. Note that most of the data points in Figs. 8 and 10 are based on four separate differential cross sections. Typically two spectroscopic transitions are available for one rotational state and two rotational states form a parity pair.

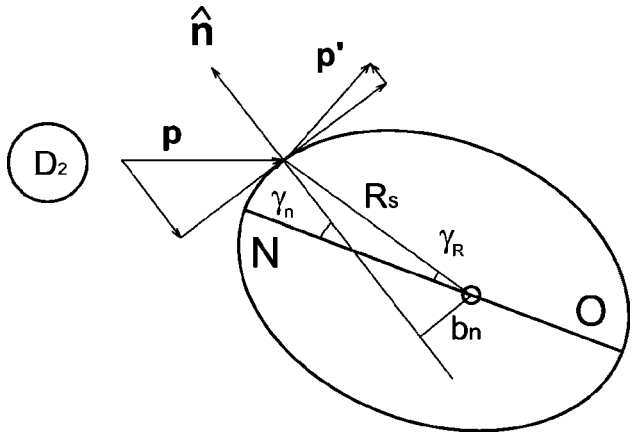


FIG. 9. Schematic representation of a hard ellipsoid NO shell colliding with a $D_2$ molecule. The incoming linear momentum $p$ is decomposed into a component parallel and one perpendicular to the hard shell. The parallel component is conserved during collision, while the perpendicular one is partly transferred into rotation.

The observation that $D_2$–NO collisions yield more forward scattering than He–NO collisions could indicate a more anisotropic interaction potential. On the other hand, ion images for $\Delta j>12.5$ could not be obtained, as their cross sections were too small for both He–NO and $D_2$–NO. This opposes the explanation of a larger anisotropy causing more forward scattering for $D_2$–NO: larger anisotropy would allow classically for a larger $\Delta j$. No PESs are available for $D_2$–NO collisions, but detailed PESs are available for He–NO collisions.[28] Inspection of the $V_{\mathrm{sum}}$ contour plot in Ref. 29 gives (at $E=500$ cm$^{-1}$) for a collision onto the N-end $B=4.40a_0$, $A_{\mathrm{N}}=5.65a_0$ and for a collision onto the O-end $A_{\mathrm{O}}=5.25a_0$. To estimate the difference in anisotropy between the He–NO and $D_2$–NO potentials, Eq. (9) has been fitted to the experimental data for spin-orbit conserving collisions in Fig. 8. For now we approximate $\Delta J\approx j'+\epsilon'/2$. This fit yields for He–NO $(A-B)_{\mathrm{He-NO}}=0.76a_0$ and for $D_2$–NO $(A-B)_{\mathrm{D_2-NO}}=0.93a_0$. The $(A-B)$ values from this rough estimation are not too far away from the values derived from the *ab initio* potential. However, from this simple (classical) view, one would assume that double rainbows are present: recall that there is a maximum of $b_n$ on both the N-end and the O-end of the NO molecule. Such double maxima were indeed observed for Ne–CO scattering[30,31] and attributed to

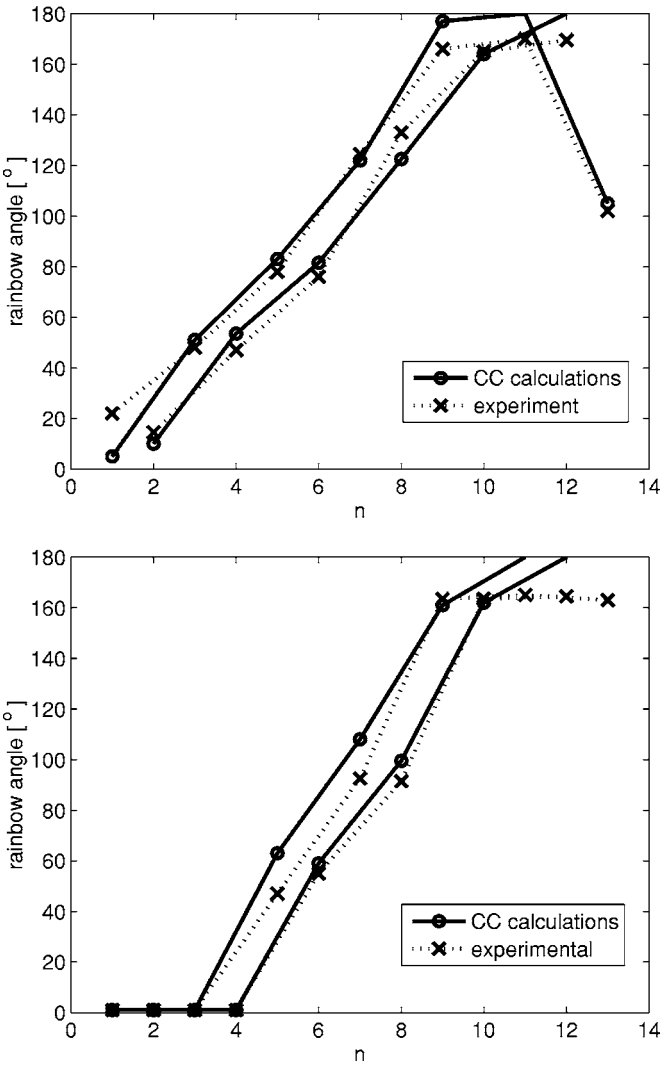


FIG. 10. Experimental He–NO rainbow maxima from Fig. 8 are compared to values from CC calculations (Ref. 18). Results for spin-orbit conserving transitions are found in the upper panel, while the lower panel shows results for spin-orbit changing transitions. The maxima for parity changing transitions ($j'+\epsilon'/2$=odd) are at larger scattering angles than those for parity conserving transitions ($j'+\epsilon'/2$=even). To elucidate this, separate lines are drawn that connect the data points for both cases. The filtering of the data causes a slight underestimation of the scattering angle with maximum differential cross section when it is close to 180°.

this effect, but remain absent in the present work. The Ne–CO system is more asymmetric than He–CO. The difference between the C and O end in the Ne–CO potential is much larger than the difference between the N and the O end in the He–NO potential.

Westley *et al.*[20] did not observe double maxima for $D_2$–NO and He–NO scattering (note that both components of the Λ doublet were present in the incoming NO beam) and concluded that the asymmetry was too small to resolve these two rainbows. From the current results, however, one would expect that their differential cross sections contain four maxima, not only one for each side of the molecule, but also for the parity conserving component and the parity changing component. If both components of the Λ doublet are present before collision, one cannot distinguish between parity changing and parity conserving transitions (for example $j=1/2$, $\epsilon=1\rightarrow j'=13/2$, $\epsilon'=1$ and $j=1/2$, $\epsilon=-1\rightarrow j'=13/2$, $\epsilon'=1$ show up in the same ion image). Equation (3) shows that both curves with labels $n=6$ and $n=7$ contribute to the same ion image when both components of the Λ doublet of $j=1/2$ are populated before collision. From Fig. 8 it becomes clear that the maxima in the cross section of the two contributing curves can be far (>40°) apart from each other.

In Fig. 10 the experimentally observed maxima for He–NO scattering are compared to those obtained in CC calculations.[18] In this figure, the points for parity changing transitions ($n$=odd) are connected by a line (for reasons of clarity) as are those for parity conserving ($n$=even) transitions. We conclude that parity changing transitions show a more forward scattered maximum of the cross section than parity conserving ones. The molecule appears to be less anisotropic for parity changing collisions than for parity conserving ones.

In contrast to Westley *et al.*,[20] we observe that the $D_2$–NO maxima of the differential cross section are substantially more forward scattered than those of He–NO in the case of spin-orbit changing transitions (see Figs. 8 and 10). For both He–NO and $D_2$–NO the spin-orbit changing collisions $\vartheta_m$ remains small up to a large value of $n$, after which the differential cross section changes to completely backward scattering very rapidly. It is impossible to fit such a curve using Eq. (9). Overall we conclude that spin-orbit changing collisions at the same value of $n$ turn out to be more forward scattered than in the case of spin-orbit conserving transitions.

## IV. CONCLUDING REMARKS

Differential cross sections for fully quantum state selected NO molecules ($j=1/2$, $\Omega=1/2$, $\epsilon=-1$) colliding with $D_2$ are obtained using the velocity-mapped ion-imaging technique. The detection step is fully quantum state resolved ($j',\Omega',\epsilon'$), which allows for an investigation of the effect of changing and conservation of parity on the differential cross section. The $D_2$–NO differential cross sections for various final states are plotted in Figs. 3–5. In both the spin-orbit conserving and changing cases, He–NO collisions show maxima of the differential cross sections at larger scattering angles than those found in the present study ($D_2$–NO). This possibly could indicate a larger anisotropy of the $D_2$–NO shell compared to the He–NO potential, but this would also allow for excitation to higher rotational states which is not observed.

Parity pairs are observed in the differential cross sections for both spin-orbit conserving and spin-orbit changing collisions. The present results show a significant difference between differential cross sections for scattering into the upper and lower components of the Λ doublet of NO. The angular dependence of the cross sections is found to depend on the parity pair number $n=j'-\epsilon\epsilon'/2$. For excitation to pairs of neighboring $j'$ states with the same parity, the angular dependence of the cross section turns out to be similar, which indicates that the differential cross section is proportional.

It was shown that there exists a large difference between maxima (rainbow positions) for parity conserving and for

parity changing transitions. If no full (hexapole) state selection is applied, four rotational rainbows may contribute to the differential cross sections: two for scattering from both sides of the molecule, one for parity conserving transitions, and one for parity changing transitions. This should be explored in future experimental studies with the aim to observe the four maxima separately. Parity propensity rules are expected to become less pronounced with increasing anisotropy of the interaction potential.

## ACKNOWLEDGMENTS

The authors congratulate Yuan Lee on his 70th birthday and thank him for his pioneering and inspiring work in the field of molecular dynamics. The Netherlands Organization for Scientific Research (NWO) is gratefully acknowledged for financial support through CW and FOM. The authors are very grateful to Professor A. W. Kleyn for his experimental support.

[1] D. M. Neumark, A. M. Wodtke, G. N. Robinson, C. C. Hayden, and Y. T. Lee, J. Chem. Phys. **82**, 3045 (1985).
[2] H. Kohguchi, T. Suzuki, and M. H. Alexander, Science **294**, 832 (2001).
[3] R. D. Levine, *Reaction Dynamics* (Cambridge University Press, Cambridge, 2005).
[4] D. W. Chandler and P. L. Houston, J. Chem. Phys. **87**, 1445 (1987).
[5] A. T. J. B. Eppink and D. H. Parker, Rev. Sci. Instrum. **68**, 3477 (1997).
[6] *Imaging in Molecular Dynamics*, edited by B. Whitaker (Cambridge University Press, Cambridge, 2003).
[7] N. Yonekura, C. Gebauer, H. Kohguchi, and T. Suzuki, Rev. Sci. Instrum. **70**, 2365 (1999).
[8] A. A. Dixit, P. J. Pisano, and P. L. Houston, J. Phys. Chem. A **105**, 11165 (2001).
[9] K. T. Lorenz, D. W. Chandler, J. W. Barr, W. Chen, G. L. Barnes, and J. I. Cline, Science **293**, 2063 (2001).
[10] M. S. Elioff, J. J. Valentini, and D. W. Chandler, Science **302**, 1940 (2003).
[11] T. P. Rakitzis, A. J. van den Brom, and M. H. M. Janssen, Science **303**, 1852 (2004).
[12] M. H. Alexander and S. Stolte, J. Chem. Phys. **112**, 8017 (2000).
[13] J. L. van Leuken, J. Bulthuis, S. Stolte, and J. G. Snijders, Chem. Phys. Lett. **260**, 595 (1996).
[14] M. J. L. de Lange, M. Drabbels, P. T. Griffiths, J. Bulthuis, and J. G. Snijders, Chem. Phys. Lett. **313**, 491 (1999).
[15] A. E. Wiskerke, C. A. Taatjes, A. W. Kleyn, R. J. W. E. Lahaye, S. Stolte, D. K. Bronnikov, and B. E. Hayden, Faraday Discuss. **96**, 297 (1993).
[16] K. H. Kramer and R. B. Bernstein, J. Chem. Phys. **40**, 200 (1964).
[17] M. G. Tenner, E. W. Kuipers, W. Y. Langhout, A. W. Kleyn, G. Nicolasen, and S. Stolte, Surf. Sci. **236**, 151 (1990).
[18] A. Gijsbertsen, H. Linnartz, G. Rus, A. E. Wiskerke, S. Stolte, D. W. Chandler, and J. Klos, J. Chem. Phys. **123**, 224305 (2005).
[19] A. Gijsbertsen, S. Stolte, H. Linnartz, and C. A. Taatjes, J. Am. Chem. Soc. **128**, 8777 (2006).
[20] M. S. Westley, K. T. Lorenz, D. W. Chandler, and P. L. Houston, J. Chem. Phys. **2**, 473 (2001).
[21] M. S. Child, *Molecular Collision Theory* (Dover, Mineola, NY, 1996).
[22] U. Beck, U. Ross, and W. Schlepper, Z. Phys. A **293**, 107 (1979).
[23] S. Bosanac, Phys. Rev. A **22**, 2617 (1980).
[24] S. Bosanac and U. Buck, Chem. Phys. Lett. **81**, 315 (1981).
[25] H. J. K. R. Schinke, J. Chem. Phys. **73**, 1222 (1980).
[26] J. M. Bowman and K. T. Lee, J. Chem. Phys. **74**, 2664 (1981).
[27] H. J. K. R. Schinke, J. Chem. Phys. **75**, 3850 (1981).
[28] J. Klos, G. Chalasinski, M. T. Berry, R. Bukowski, and S. M. Cybulski, J. Chem. Phys. **112**, 2195 (2000).
[29] M. J. L. de Lange, S. Stolte, C. A. Taatjes, J. Klos, G. C. Groenenboom, and A. v. d. Avoird, J. Chem. Phys. **121**, 11691 (2004).
[30] K. T. Lorenz, D. W. Chandler, and G. C. McBane, J. Phys. Chem. A **106**, 1144 (2002).
[31] G. C. McBane and S. M. Cybulski, J. Chem. Phys. **110**, 11734 (1999).
[32] M. J. L. de Lange, Ph.D. thesis, Vrije Universiteit Amsterdam, 2003.
[33] Hund's case (a) coupling dominates (Ref. 32) for the achievable final rotational states of NO here. Labels $\bar{\Omega}'=1/2$ and $\bar{\Omega}'=3/2$ correspond to scattering into the $F_1$ and $F_2$ levels.
[34] See EPAPS Document No. E-JCPSA6-125-145637 for tables with measured $D_2-NO$ differential cross sections. The experimental differential cross section for each final state is provided as function of the center-of-mass scattering angle at each degree to facilitate comparison to eventual theoretical values. This document can be reached via a direct link in the online article's HTML reference section or via the EPAPS homepage (http://www.aip.org/pubservs/epaps.html).